Synthetic study of wide-azimuth AVO analysis with anisotropic spreading correction

Xiaoxia Xu and Ilya Tsvankin
Center for Wave Phenomena, Department of Geophysics, Colorado School of Mines, Golden, CO 80401

ABSTRACT

In azimuthal AVO (amplitude-variation-with-offset) analysis, it is common to compensate for geometrical spreading by applying empirical amplitude gain corrections that may give erroneous results when the overburden is azimuthally anisotropic. Here, we present a synthetic modeling study where we test a more rigorous, moveout-based anisotropic spreading correction (MBASC) on PP reflections from the bottom of an orthorhombic layer.

The wide-azimuth, long-offset data were computed by the anisotropic reflectivity method, which generates exact wavefields for a stack of horizontal, azimuthally anisotropic layers. Although the MBASC algorithm is valid within the framework of ray theory and does not account for the transmission through the top of the target layer, it accurately reconstructs the reflection coefficient for a wide range of offsets and azimuths. Errors in the estimated reflection coefficient are mostly caused by the intereference of the target event with shear and mode-converted waves.

We also examined the performance of the empirical t^2-gain correction on three models with different relative strength of the azimuthal variation of the geometrical spreading. If the azimuthal dependence of the reflection coefficient is much more pronounced (i.e., three times or more at an angle of 20°) than that of the geometrical spreading, the t^2-correction can be used for purposes of qualitative azimuthal AVO analysis. However, when this condition is not satisfied, the empirical correction distorts or even obliterates (the case of our model 3) the azimuthal AVO signature. Also, quantitative inversion of the azimuthal AVO response for all three models requires application of the more rigorous MBASC method.

This work confirms that our geometrical-spreading correction can efficiently handle strongly anisotropic overburden that may include layers of orthorhombic symmetry. It should be emphasized that the MBASC method operates with the effective moveout parameters derived directly from wide-azimuth traveltimes and does not need any other information about the velocity model.

Key words: Geometrical-spreading correction, azimuthal anisotropy, wide-azimuth AVO, nonhyperbolic moveout, reflectivity modeling

Introduction

Since amplitude-variation-with-offset analysis is designed for the plane-wave reflection coefficient at the target horizon, AVO inversion has to include compensation for the amplitude loss in the overburden. For homogeneous non-attenuative isotropic media, the amplitude decay (geometrical spreading) is proportional to the distance or traveltime from the source to the receiver. Although the geometrical-spreading factor becomes much

more complicated in the presence of anisotropy and/or heterogeneity, the simple t-gain is often used in practice to enhance later arrivals (Yilmaz, 2001). Another common gain factor, t^2, describes the amplitude decay in homogeneous isotropic media with constant attenuation (Claerbout, 1985). Such semi-empirical amplitude corrections, however, may not be sufficiently accurate for realistic subsurface models.

The azimuthal AVO signature measured over fractured reservoirs is used to identify the dominant fracture directions and, in some cases, estimate the crack density (Hall and Kendall, 2003; Gray and Todorovic-Marinic, 2004). If the overburden is azimuthally anisotropic, the AVO response for wide-azimuth data can be significantly distorted by the anisotropic geometrical spreading and, possibly, by the transmission coefficients along the raypath. Although the strong influence of the anisotropic overburden on the amplitudes of reflected waves has been discussed in the literature (Tsvankin, 2005; Xu et al., 2005), azimuthal AVO analysis still employs conventional amplitude-compensation corrections.

To remove the geometrical-spreading factor from the azimuthal AVO response, Xu et al. (2005) and Xu and Tsvankin (2006) proposed a moveout-based anisotropic spreading correction method that we will call "MBASC." This method makes it possible to compute geometrical spreading for wide-angle reflected waves in horizontally-layered, azimuthally anisotropic media from the reflection traveltimes. The spreading correction is preceded by 3D nonhyperbolic moveout inversion based on the global-semblance algorithm of Vasconcelos and Tsvankin (2006). The moveout parameters, estimated from long-offset, wide-azimuth data, serve as the input to the geometrical-spreading correction. MBASC does not require knowledge of the velocity model (except for the subsurface layer) and was shown to be robust in the presence of noise (for details, see Xu et al., 2005, and Xu and Tsvankin, 2006).

Here, we test the MBASC algorithm on synthetic wide-azimuth P-wave data generated by the anisotropic reflectivity method. Since the modeling code computes exact 3D amplitudes, this numerical study helps to evaluate the impact of two limitations of our methodology. First, MBASC is based on the zero-order ray theory (i.e., on the leading term of the ray-series expansion), which is known to produce amplitude distortions even for structurally simple anisotropic media (Tsvankin, 2005). Second, our algorithm does not account for the transmission coefficients along the raypath. Another practically important issue addressed here is whether MBASC can be replaced by empirical gain corrections in azimuthal AVO analysis. We start by describing the modeling code and the algorithm used to reconstruct the reflection coefficient from the picked amplitudes of the reflected waves. Then we compare the performance of MBASC and the t^2-gain correction for three models that include an orthorhombic layer beneath an isotropic overburden.

Synthetic modeling

The modeling algorithm, based on the anisotropic version of the so-called reflectivity method, is designed to simulate exact 3D wavefields for horizontally layered anisotropic media (Fryer and Frazer, 1984; Chin et al., 1994). The reflectivity code (ANISYNPA) was originally developed by Corrigan (1990) and later modified at the Center for Wave Phenomena.

All three models used here include an orthorhombic layer sandwiched between two isotropic layers (see Tables 1, 2, and 3). One of the symmetry planes of the orthorhombic medium is horizontal, while the other two coincide with the coordinate planes $[x_1, x_3]$ (azimuth 0°) and $[x_2, x_3]$ (azimuth 90°). Synthetic seismograms were computed for a wide range of offsets in both vertical symmetry planes, as well as for the 45°-azimuth. The code calculates three displacement components of the wavefield excited by a point force aligned with one of the coordinate axes.

The vertical displacement from a vertical force for the three models is displayed in Figures 1–3. Our goal is to carry out azimuthal AVO analysis for the PP-wave reflected from the bottom of the orthorhombic layer (marked by arrows in Figures 1–3). To avoid the interference of this PP reflection with ground roll and surface-related multiples, we eliminated the free surface in the computation of the synthetic seismograms. Still, the target PP event interferes with the PS- and SS-wave reflections from the top of the orthorhombic layer (the ellipses in Figures 1–3), which causes distortions of the picked AVO response.

Estimation of the reflection coefficient from the AVO response

The moveout-based anisotropic geometrical-spreading correction described in Xu and Tsvankin (2006) was implemented for layered orthorhombic media in the Seismic Unix (SU; Stockwell, 1997) program "suazavo." The MBASC code computes the offset- and azimuth-dependent geometrical-spreading factor for a given reflection event using the zero-offset time t_0 and effective moveout parameters $V_{\rm nmo}^{(1)}$, $V_{\rm nmo}^{(2)}$, $\eta^{(1)}$, $\eta^{(2)}$, and $\eta^{(3)}$. The symmetry-plane normal-moveout (NMO) velocities $V_{\rm nmo}^{(1)}$ and $V_{\rm nmo}^{(2)}$ determine the NMO ellipse on conventional spreads, while the anellipticity parameters $\eta^{(1)}$, $\eta^{(2)}$, and $\eta^{(3)}$ control nonhyperbolic (long-spread) moveout. The moveout parameters are estimated with the 3D algorithm of Vasconcelos and Tsvankin (2006), which maximizes semblance computed for all offsets and azimuths in the gather. It should be emphasized that the geometrical-spreading correction is not influenced

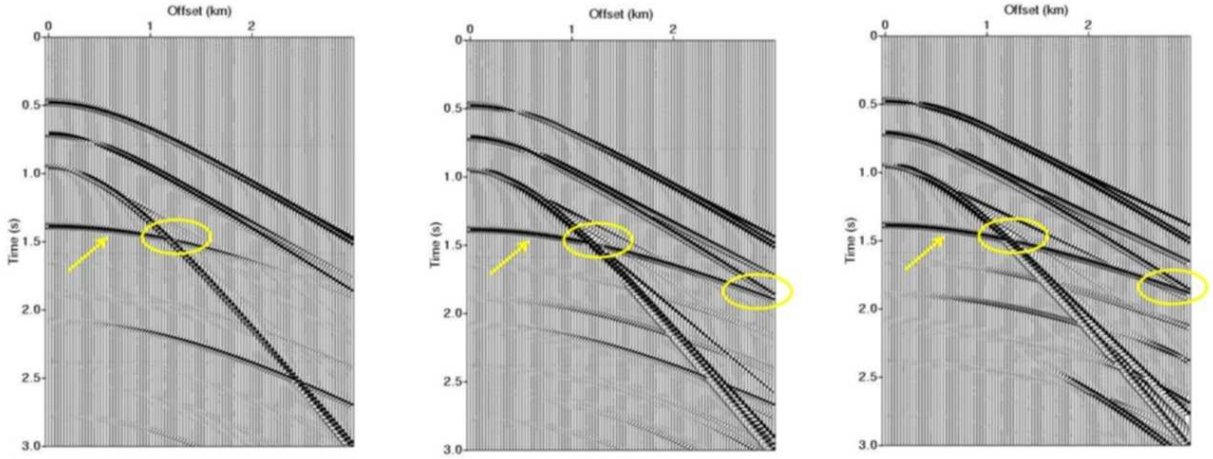

Figure 1. Synthetic gathers for model 1 (Table 1) computed by the reflectivity method in three azimuthal directions: (a) 0° (symmetry plane $[x_1, x_3]$); (b) 45°; and (c) 90° (symmetry plane $[x_2, x_3]$). The top layer is specified as a halfspace to eliminate the influence of the free surface. The arrows mark the target PP-wave reflected from the bottom of the orthorhombic layer. The ellipses highlight the areas of interference of the target PP event with the PS and SS reflections from the top of the orthorhombic layer.

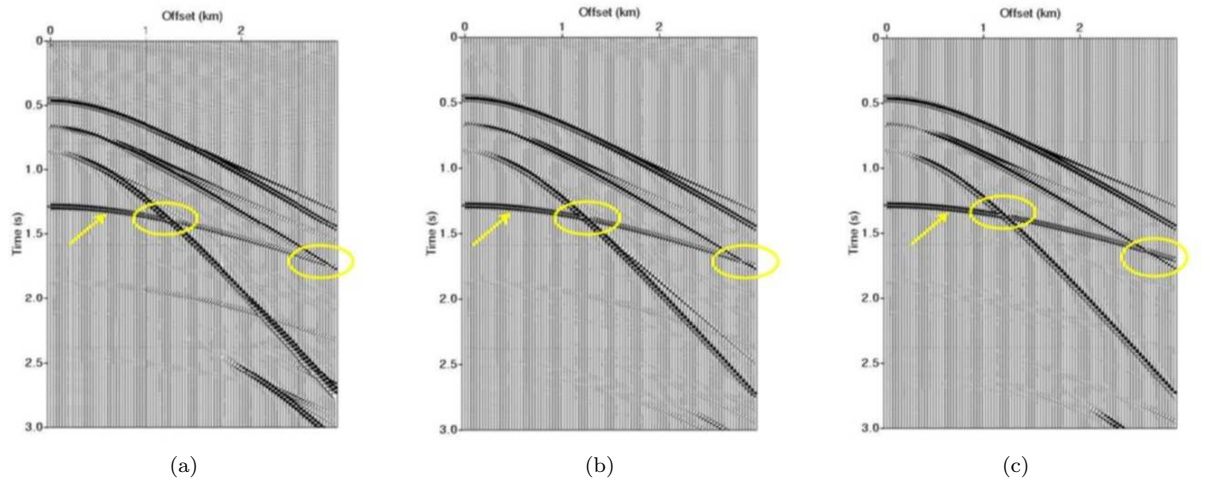

Figure 2. Synthetic gathers for model 2 (Table 2) in three azimuthal directions: (a) 0° (symmetry plane $[x_1, x_3]$); (b) 45°; and (c) 90° (symmetry plane $[x_2, x_3]$).

by the trade-offs between the NMO velocities and η-parameters, as long as the reconstructed moveout function is sufficiently close to the actual traveltimes.

The processing flow starts with picking the raw amplitudes of a certain event on all traces along the traveltime surface defined by the estimated moveout parameters. Then the picked amplitudes are corrected for the anisotropic geometrical spreading computed for each offset and azimuth. Finally, assuming that the sources and receivers are located in an isotropic layer with a known P-wave velocity, the algorithm removes the source and receiver directivity factors using local time slopes (i.e., the horizontal slownesses) calculated from the moveout function.

Since our models are non-attenuative, the spatial variation of the corrected amplitude should be determined primarily by the plane-wave reflection coefficient. The only propagation factor not accounted for in this algorithm is the product of the transmission coefficients along the raypath, which is usually close to unity (see

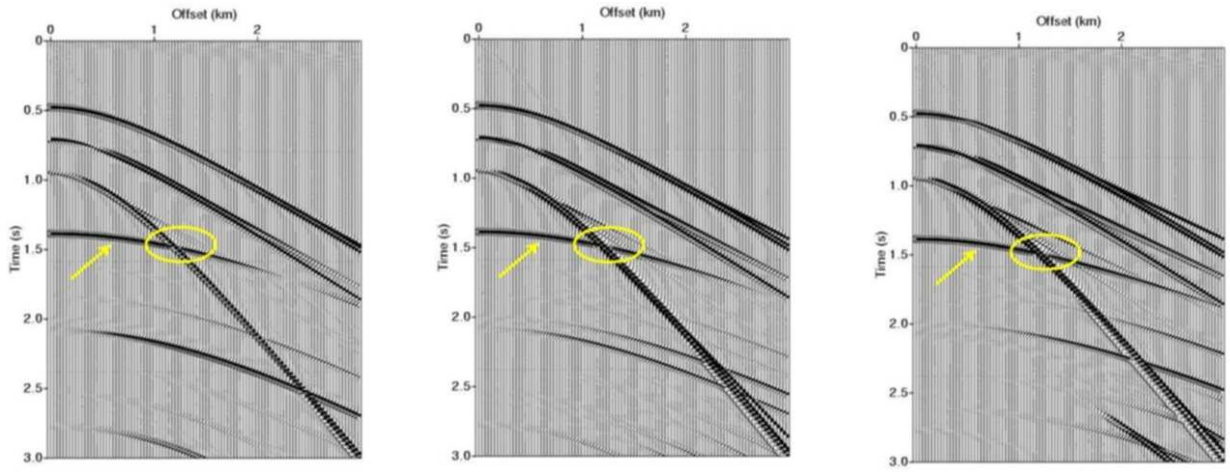

Figure 3. Synthetic gathers for model 3 (Table 3) in three azimuthal directions: (a) 0° (symmetry plane $[x_1, x_3]$); (b) 45°; and (c) 90° (symmetry plane $[x_2, x_3]$).

below). A constant multiplier related to the strength of the source can be removed by simple normalization.

The output amplitudes have to be smoothed to mitigate the distortions caused by the interference of the PP reflection with shear and converted waves (see the ellipses in Figures 1–3). The smoothing was accomplished by least-squares fitting of a fourth-order polynomial in the horizontal slowness to the reconstructed reflection coefficients. In practice, the results of AVO processing often require smoothing because of noisy amplitudes, variations in the source and receiver coupling, etc.

Model 1

Laboratory measurements for orthorhombic samples of sedimentary rocks are relatively rare (Sarkar et al, 2003; Mah and Schmitt, 2003). Therefore the parameters of the orthorhombic layer in model 1 (see Table 1) are based on laboratory measurements for two brine-saturated TI (transversely isotropic) shale samples (Wang, 2002). The main reason for choosing this set of parameters is that the large difference between the parameters $\gamma^{(1)}$ and $\gamma^{(2)}$ causes an extremely pronounced azimuthal variation of the P-wave AVO gradient (Rüger, 2001). Note that $\gamma^{(1)} = 0.513$ is much higher that the average value for shales in Wang's (2002) table (0.2), so this model likely exaggerates the typical magnitude of the azimuthal AVO response.

The PP-wave reflection coefficient from the bottom of the orthorhombic layer reconstructed by our algorithm (i.e., using the moveout-based geometrical-spreading correction) is shown in Figure 4a (dashed lines). The maximum horizontal slowness (0.3 s/km) corresponds to an incidence angle at the source close to 40° (it varies with azimuth) and an offset-to-depth-ratio slightly larger than two. The slownesses up to 0.15 s/km (the incidence angle close to 20°) define what we will call the near-offset amplitude response; the reflection coefficient for this slowness range is governed mostly by the AVO gradient.

For comparison, we also plot in Figure 4a the exact reflection coefficient (solid lines) calculated using the algorithm of Jílek (2002). To remove the source factor, the estimated reflection coefficient is normalized to match the exact value at normal incidence (zero offset). Clearly, for near offsets our algorithm recovers the reflection coefficient with extremely high accuracy. The small deviation of the estimated reflection coefficient from the exact curve at far offsets for azimuths of 45° and 90° is related to the interference with shear and mode-converted waves (Figures 1b and 1c).

The excellent agreement between the reconstructed and exact reflection coefficients for a wide range of offsets and azimuths is ensured by the application of the moveout-based geometrical-spreading correction. Figure 5 confirms that the output of MBASC for all three azimuths practically coincides with the geometrical spreading computed by dynamic ray tracing.

In addition to confirming the high accuracy of the MBASC algorithm, it is important to evaluate the performance of simple empirical gain corrections often used in practice. Here, we present only the amplitudes corrected by the t^2-function (Figure 4b), which generally gives better results for our models than the linear t-compensation. For an azimuth of 0° the reflection coefficient after application of the t^2-gain is close to the exact value for the full offset range. The accuracy of the

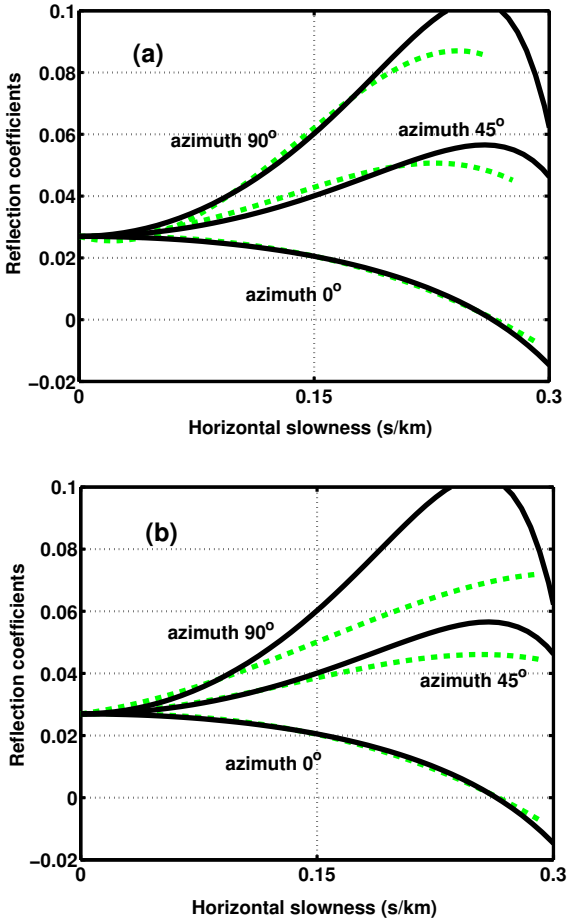

Figure 4. Comparison of the reconstructed (dashed lines) and exact (solid lines) reflection coefficients for the PP-wave reflected from the bottom of the orthorhombic layer in model 1. The reflection coefficient is estimated using (a) the MBASC method; and (b) the t^2-gain. The offset-to-depth ratio that corresponds to the maximum horizontal slowness (0.3 s/km) is slightly larger than two.

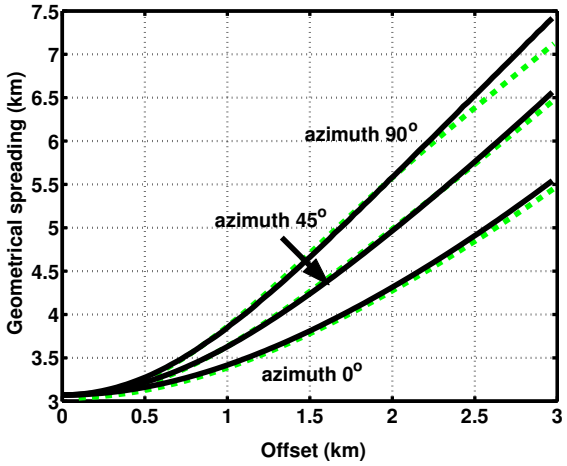

Figure 5. Comparison of the geometrical spreading computed by the MBASC method (dashed lines) and dynamic ray tracing (solid) for the PP reflection from the bottom of the orthorhombic layer in model 1.

reconstructed coefficient, however, is much lower for the other two azimuths, especially at far offsets.

Since the traveltime depends on both polar and azimuthal velocity variations, the t^2-function absorbs some of the influence of the anisotropy on the geometrical-spreading factor. As illustrated in Figure 4b, while the t^2-gain happens to be adequate for the 0°-azimuth, it does not accurately reproduce the the anisotropic geometrical spreading away from that direction. Still, it is clear from Figures 4a and 4b that the t^2-correction may be sufficient for purposes of qualitative azimuthal AVO analysis. For model 1, the magnitude of the azimuthal variation of the AVO gradient is so pronounced that the influence of errors in the geometrical-spreading factor becomes insignificant. Quantitative inversion of the AVO response on long-spread gathers, however, should be based on the MBASC algorithm.

Model 2

The parameters of the orthorhombic layer in model 2 are typical for a set of parallel, vertical, penny-shaped cracks embedded in a VTI (transversely isotropic with a vertical symmetry axis) background medium (Schoenberg and Helbig, 1997). The reflection coefficient for the PP reflection from the bottom of the orthorhombic layer computed by our method remains accurate up to a horizontal slowness of about 0.2 s/km (Figure 6a). Note that for model 2 the slowness 0.15 s/km corresponds to an incidence angle close to 25° (slightly higher than that for model 1) and an offset-to-depth ratio of one. At far offsets, the reconstructed reflection coefficient is severely distorted by the interference of the target event with the PS conversion from the top of the orthorhombic layer (see Figure 2).

The output of the t^2-gain correction for this model is less accurate compared to model 1 (Figure 6b). For all three azimuths, the reflection coefficient after the t^2-correction is larger than the exact value, and the error becomes noticeable at relatively small offsets. For the 90°-azimuth, the reconstructed reflection coefficient even has the wrong sign of the AVO gradient. However, while t^2-gain is clearly inadequate for purposes of the AVO inversion, it correctly reproduces the azimuthal trend of the AVO gradient between the vertical symmetry planes.

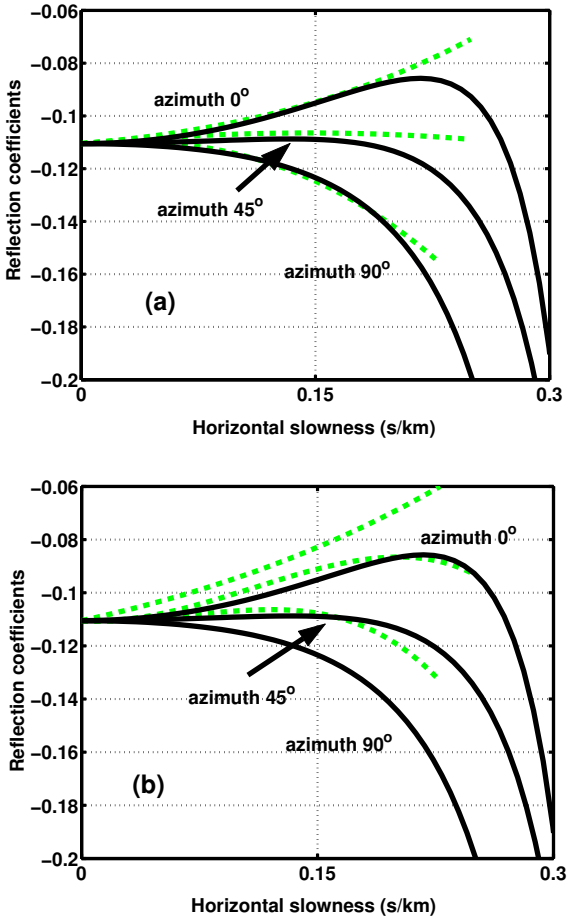

Figure 6. Comparison of the reconstructed (dashed lines) and exact (solid) reflection coefficients for model 2. The reflection coefficient is estimated using (a) the MBASC method; and (b) the t^2-gain. The offset-to-depth ratio that corresponds to the maximum horizontal slowness (0.3 s/km) is close to 2.5.

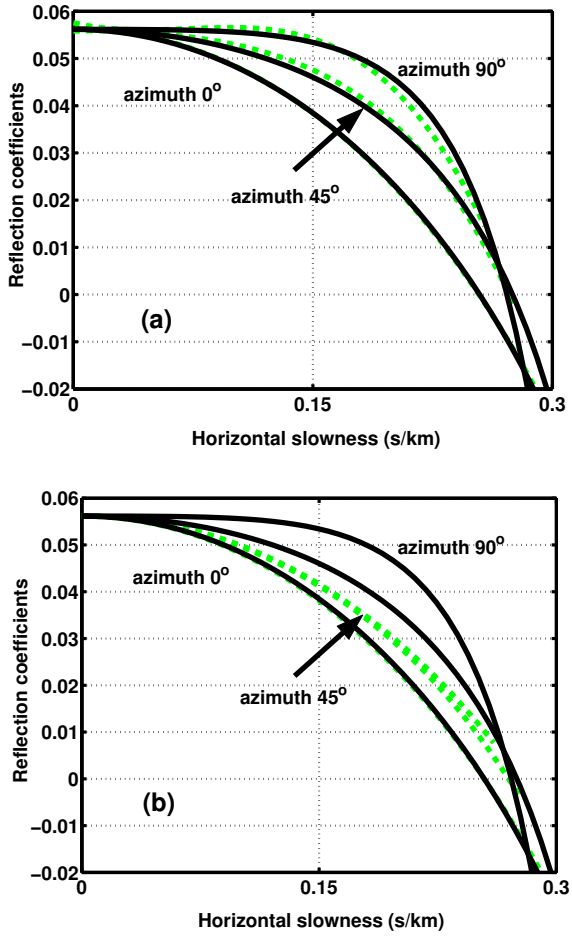

Figure 7. Comparison of the reconstructed (dashed lines) and exact (solid) reflection coefficients for model 3. The reflection coefficient is estimated using (a) the MBASC method; and (b) the t^2-gain. The reconstructed reflection coefficients for the 45°- and 90°-azimuths on plot (b) almost coincide with one another; for the 0°-azimuth, the reconstructed and exact coefficients are practically identical. The offset-to-depth ratio that corresponds to the maximum horizontal slowness (0.3 s/km) is close to two.

Model 3

The last model is designed in such a way that the geometrical spreading of the target event from the bottom of the orthorhombic layer is the same as that in model 1, but the azimuthal variation of the reflection coefficient is much less pronounced. Because of the high accuracy of the MBASC method (Figure 5) and the absence of interference with other arrivals at large offsets, the recovered and exact reflection coefficients are almost identical for the whole range of offsets and azimuths (Figure 7a).

The impact of the errors produced by the t^2-gain in this model is amplified by the relatively weak azimuthal dependence of the reflection coefficient (Figure 7b). The ratio of the azimuthal variation of the geometrical spreading and that of the reflection coefficient (estimated at a horizontal slowness of 0.15 s/km) increases from 5% for model 1 to 40% for model 3. The reflection coefficients after the t^2-gain are close for all three azimuths (and practically coincide for 0° and 90°, even at far offsets. Evidently, such small azimuthal differences in amplitude would be undetectable in the presence of realistic noise. Hence, application of the empirical t^2-correction for this model practically removes the azimuthal AVO signature typically associated with natural fractures.

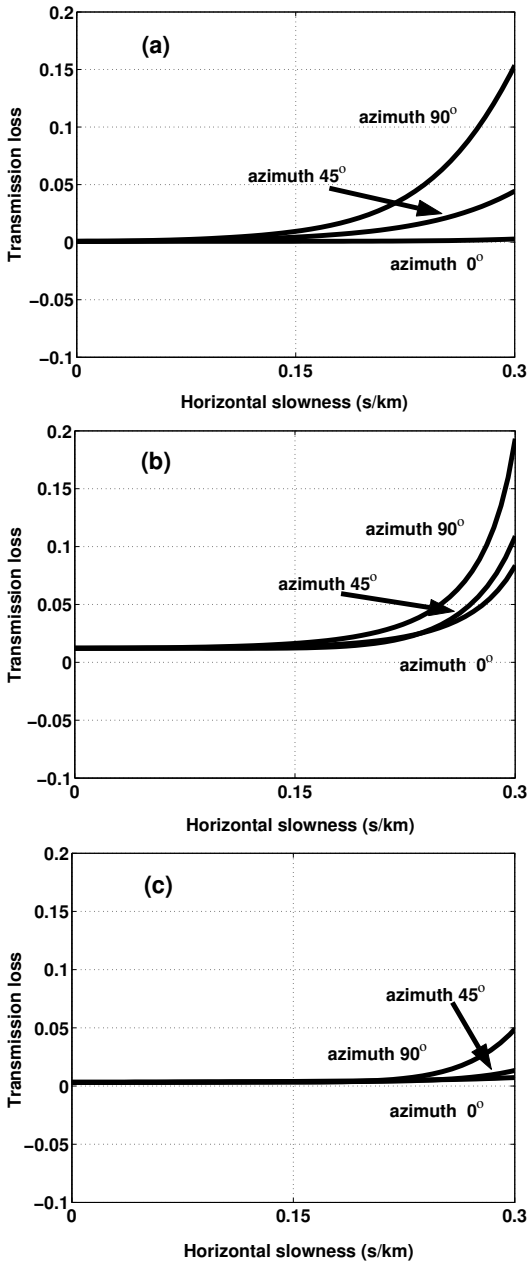

Figure 8. Transmission loss for the PP reflection from the bottom of the orthorhombic layer in (a) model 1; (b) model 2; and (c) model 3. The loss is computed by subtracting from unity the product of the plane-wave transmission coefficients along the raypath.

Influence of the transmission loss

The transmission coefficients along the raypath are not part of the geometrical-spreading correction, and it is difficult to estimate them from surface data. To evaluate the transmission loss for our models, we subtract from unity the product of the transmission coefficients along the raypath of the target PP reflection (Figure 8). For all three models, the transmission loss becomes noticeable only at far offsets, but the related azimuthal amplitude variation is much smaller than that of the reflection coefficients (e.g., compare Figure 8a with the solid curves in Figure 4). Therefore, the transmission loss can be considered a secondary factor in azimuthal AVO analysis, which is confirmed by our results discussed above and by the observations of Maultzsch et al. (2003).

Conclusions

The transformation of seismic amplitudes measured at the surface into the reflection coefficient at the target horizon is a critically important step in AVO analysis. Here, we tested the moveout-based geometrical-spreading correction (MBASC) on long-offset, wide-azimuth synthetic data from three models that included a strongly anisotropic layer of orthorhombic symmetry. The reflectivity method used to compute the synthetic seismograms generates exact 3D wavefields for horizontally layered media.

One potential limitation of the MBASC method is its reliance on ray-theory relationships between the traveltime derivatives and reflection amplitudes. Also, any geometrical-spreading correction does not include compensation for the transmission coefficients along the raypath. However, our synthetic study shows that despite these limitations, MBASC accurately reconstructs the azimuthally varying reflection coefficient for a wide range of offsets and azimuths. The errors in the estimated reflection coefficient are largely caused by interference-related amplitude distortions of the target event. Most importantly, the moveout-based correction operates just with reflection traveltimes and does not require knowledge of the velocity model.

In practice, azimuthal AVO analysis is often preceded by an empirical gain correction designed to approximately compensate for the amplitude loss in the overburden. Our tests demonstrate that although the t^2-gain absorbs some of the influence of anisotropy on geometrical spreading, it produces significant errors in the reflection coefficient, especially for offsets-to-depth ratios greater than unity. Therefore, the empirical correction cannot be used in quantitative inversion of the azimuthally varying AVO response for the anisotropy parameters (e.g., for the fracture compliances).

On the other hand, most existing applications of azimuthal AVO can be called "qualitative" because they are based on estimating the principal azimuthal directions of the AVO gradient and its variation between the vertical symmetry planes. This relative azimuthal change in the AVO gradient measured over a fractured reservoir is then used to identify "sweet spots" of high fracture density. For models where the azimuthal variation of the reflection coefficient is much more pro-

nounced than that of geometrical spreading (e.g., our models 1 and 2), the t^2-gain can reproduce the general azimuthal trend of the reflection coefficient. However, as the ratio of the azimuthal variation of the geometrical spreading and that of the reflection coefficient (estimated at a horizontal slowness of 0.15 s/km) increases from 5% in model 1 to 40% in model 3, the empirical correction smears the AVO signature. For model 3, the reflection coefficient after the t^2-correction is so weakly dependent on azimuth that it contains almost no information about the underlying azimuthally anisotropic model.

Discussion

In our synthetic study, we processed long-offset reflection data that help to increase the sensitivity of the azimuthal AVO response to the anisotropy (e.g., fracture) parameters. However, even if amplitude analysis is restricted to the AVO gradient estimated on near offsets, the MBASC method can benefit from nonhyperbolic moveout inversion for the anellipticity parameters $\eta^{(1)}$ and $\eta^{(2)}$. Indeed, according to equation 30 of Xu et al. (2005), the azimuthal variation of geometrical spreading at near offsets is governed by the parameter combination $3(\eta^{(1)} - \eta^{(2)}) - (\delta^{(1)} - \delta^{(2)})$. The presence of the η-parameters in this expression is explained by the high sensitivity of geometrical spreading to the second traveltime derivative with respect to phase angle or offset (Tsvankin, 2005). In principle, the contribution of the parameters $\eta^{(1)}$ and $\eta^{(2)}$ to conventional-spread moveout is partially contained in the best-fit NMO ellipse. Still, the accuracy of the reconstructed AVO gradient can be increased by applying the geometrical-spreading correction with the anellipticity parameters obtained from long-offset data.

The above modeling results show that the MBASC method becomes essential even in qualitative AVO analysis when the azimuthal variation of the geometrical spreading reaches about 1/3 of that of the reflection coefficient. It is important to mention that geometrical spreading and reflection coefficient depend on two different sets of medium parameters defined at different scales. For VTI media, this issue is discussed by Tsvankin (2005, p. 92). When the model is orthorhombic, the azimuthal variation of the P-wave AVO gradient is governed by the *local* jump in the shear-wave splitting parameter $\gamma^{(S)}$ and in the difference $\delta^{(2)} - \delta^{(1)}$ across the target interface (see equation 8.13 in Rüger, 2001). In contrast, geometrical spreading of reflected waves depends on the *effective* (average) parameters of the overburden. As discussed above, the azimuthal variation of the P-wave geometrical spreading is particularly sensitive to the difference between the effective symmetry-plane anellipticity parameters $\eta^{(1)}$ and $\eta^{(2)}$.

If the reservoir is more heavily fractured than the layer above it, the jumps in $\gamma^{(S)}$ and $\delta^{(2)} - \delta^{(1)}$ may far exceed the effective difference $\eta^{(1)} - \eta^{(2)}$ in the overburden. Then the reflection coefficient at the top of the target exhibits much larger azimuthal variations than those of the geometrical spreading. This explains why application of azimuthal AVO analysis with the conventional (isotropic) spreading correction often produces results which are in good agreement with other fracture-characterization methods (e.g., Gray and Todorovic-Marinic, 2004).

However, in many cases natural fractures that respond to the local stress field permeate the whole section and lead to substantial azimuthal anisotropy in the overburden. Also, the azimuthal variation of geometrical spreading is more significant for the reflection from the *bottom* of the reservoir, especially for relatively thick reservoir layers. As discussed by Sayers and Rickett (1997), it is generally preferable to use the reflection from the bottom of a fractured layer for fracture-characterization purposes. Finally, our tests demonstrate that *quantitative* inversion of the azimuthal AVO response for the fracture parameters cannot be carried out without a robust geometrical-spreading correction that accounts for anisotropic propagation phenomena.

Acknowledgments

We are grateful to Jyoti Behura, Rodrigo Fuck and other students and faculty at the Center for Wave Phenomena (CWP), Colorado School of Mines (CSM), for useful discussions. Dave Hale (CSM), Andreas Rüger (Landmark Graphics) and Debashish Sarkar (GX Technology) helped us to improve the reflectivity code ANISYNPA. The exact reflection coefficients were computed using software written by Petr Jílek (BP, formerly CSM). The support for this work was provided by the Consortium Project on Seismic Inverse Methods for Complex Structures at CWP and by the Chemical Sciences, Geosciences and Biosciences Division, Office of Basic Energy Sciences, Office of Science, U.S. Department of Energy.

REFERENCES

Chin, R., G. Hedstrom, and L. Thigpen, 1984, Matrix methods in synthetic seismograms: Geophysical Journal of the Royal Astronomical Society, **77**, 483–502.

Claerbout, J., 1985, Imaging the Earth's interior: available at http://www.stanford.edu/sep/jon/.

Corrigan, D., 1990, The effect of azimuthal anisotropy on the variation of reflectivity with offset: 4th International Workshop on Anisotropy.

Fryer, G. J., and L. N. Frazer, 1984, Seismic waves in stratified anisotropic media: Geophysical Journal of the Royal Astronomical Society, **78**, 691–710.

Gray, D., and D. Todorovic-Marinic, 2004, Fracture detection using 3D azimuthal AVO: CSEG Recorder, **29**, no. 10, 5–8.

Hall, S., and J. M. Kendall, 2003, Fracture characterization at Valhall: Application of P-wave amplitude variation with offset and azimuth (AVOA) analysis to a 3-D ocean-bottom data set: Geophysics, **68**, 1150–1160.

Jílek, P., 2002, Modeling and inversion of converted-wave reflection coefficients in anisotropic media: A tool for quantitative AVO analysis: Ph.D. thesis, Colorado School of Mines.

Mah, M., and D. R. Schmitt, 2003, Determination of the complete elastic stiffness from ultrasonic phase velocity measurements: Journal of Geophysical Research, **108**, ECV6 1–11.

Maultzsch, S., S. Horne, S. Archer, and H. Burkhardt, 2003, Effects of an anisotropic overburden on azimuthal amplitude analysis in horizontal transverse isotropic media: Geophysical Prospecting, **51**, 61–74.

Rüger, A., 2001, Reflection coefficients and azimuthal AVO analysis in anisotropic media: Society of Exploration Geophysicists.

Sarkar, D., A. Bakulin, and R.L. Kranz, 2003, Anisotropic inversion of seismic data for stressed media: Theory and a physical modeling study on Berea Sandstone: Geophysics, **68**, 690–704.

Sayers, C. M., and J. E. Rickett, 1997, Azimuthal variation in AVO response for fractured gas sands: Geophysical Prospecting, **45**, 165–182.

Schoenberg, M., and K. Helbig, 1997, Orthorhombic media: Modeling elastic wave behavior in a vertically fractured earth: Geophysics, **62**, 1954–1974.

Stockwell, J., 1997, Free software in education: A case study of CWP/SU: Seismic Unix: The Leading Edge, **16**, 1045–1049.

Tsvankin, I., 1997, Anisotropic parameters and P–wave velocity for orthorhombic media: Geophysics, **62**, 1292–1309.

Tsvankin, I., 2005, Seismic signatures and analysis of reflection data in anisotropic media: Elsevier Science Publ. Co., Inc (second edition).

Vasconcelos, I., and I. Tsvankin, 2006, Inversion of P-wave nonhyperbolic moveout in azimuthally anisotropic media: Methodology and field-data application: Geophysical Prospecting (in print).

Wang, Z., 2002, Seismic anisotropy in sedimentary rocks, part 2: Laboratory data: Geophysics, **67**, 1423–1440.

Xu, X., I. Tsvankin, and A. Pech, 2005, Geometrical spreading of P-waves in horizontally layered, azimuthally anisotropic media: Geophysics, **70**, D43–D53.

Xu, X., and I. Tsvankin, 2006, Anisotropic geometrical-spreading correction for wide-azimuth P-wave reflections: Geophysics (in print).

Yilmaz, Ö, 2001, Seismic data analysis (Volume I): Society of Exploration Geophysicists.

	Layer 1	Layer 2	Layer 2
Symmetry type	ISO	ORTH	ISO
Thickness (km)	0.5	1.0	∞
Density (g/cm^3)	2.1	2.1	2.12
V_{P0} (km/s)	2.1	2.2	2.3
V_{S0} (km/s)	1.05	1.1	1.15
$\epsilon^{(1)}$	0	0.317	0
$\delta^{(1)}$	0	-0.054	0
$\gamma^{(1)}$	0	0.513	0
$\epsilon^{(2)}$	0	0.121	0
$\delta^{(2)}$	0	0.046	0
$\gamma^{(2)}$	0	0.138	0
$\delta^{(3)}$	0	0.1	0
$\eta^{(1)}$	0	0.42	0
$\eta^{(2)}$	0	0.07	0
$\eta^{(3)}$	0	0.05	0

Table 1. Parameters of a three-layer medium used in the numerical tests (model 1). Orthorhombic symmetry can be fully described by the two vertical velocities (V_{P0} and V_{S0}) and seven anisotropy parameters ($\epsilon^{(1)}$, $\epsilon^{(2)}$, $\delta^{(1)}$, $\delta^{(2)}$, $\delta^{(3)}$, $\gamma^{(1)}$, and $\gamma^{(2)}$). The parameter definitions (including those of the anellipticities $\eta^{(1)}$, $\eta^{(2)}$, and $\eta^{(3)}$) are given in Tsvankin (1997, 2005). The anisotropy parameters in the vertical symmetry planes of the orthorhombic layer correspond to those measured by Wang (2002) on two brine-saturated shale samples from Africa.

	Layer 1	Layer 2	Layer 2
Symmetry type	ISO	ORTH	ISO
Thickness (km)	0.5	1.0	∞
Density (g/cm^3)	2.44	2.70	2.44
V_{P0} (km/s)	2.16	2.437	2.16
V_{S0} (km/s)	1.150	1.265	1.150
$\epsilon^{(1)}$	0	0.329	0
$\delta^{(1)}$	0	0.083	0
$\gamma^{(1)}$	0	0.046	0
$\epsilon^{(2)}$	0	0.258	0
$\delta^{(2)}$	0	-0.078	0
$\gamma^{(2)}$	0	0.182	0
$\delta^{(3)}$	0	-0.106	0
$\eta^{(1)}$	0	0.211	0
$\eta^{(2)}$	0	0.398	0
$\eta^{(3)}$	0	0.194	0

Table 2. Parameters of model 2. The orthorhombic layer corresponds to the "standard" orthorhombic model of Schoenberg and Helbig (1997), with their original parameters $\gamma^{(1)}$ and $\gamma^{(2)}$ interchanged to enhance the azimuthal variation of the reflection coefficient.

	Layer 1	Layer 2	Layer 2
Symmetry type	ISO	ORTH	ISO
Thickness (km)	0.5	1.0	∞
Density (g/cm^3)	2.1	2.1	2.12
V_{P0} (km/s)	2.1	2.2	2.3
V_{S0} (km/s)	1.05	1.1	1.15
$\epsilon^{(1)}$	0	0.317	0
$\delta^{(1)}$	0	-0.054	0
$\gamma^{(1)}$	0	0.138	0
$\epsilon^{(2)}$	0	0.121	0
$\delta^{(2)}$	0	0.046	0
$\gamma^{(2)}$	0	0.03	0
$\delta^{(3)}$	0	0.1	0
$\eta^{(1)}$	0	0.42	0
$\eta^{(2)}$	0	0.07	0
$\eta^{(3)}$	0	0.05	0

Table 3. Parameters of model 3. We modified model 1 to reduce the azimuthal variation of the reflection coefficient while keeping the geometrical-spreading factor unchanged.